New cation deficient scheelites (Sr,Ce)nWO4 (n

Andarair Gomes dos Santos, Madjid Arab, Carlson Pereira de Souza, Christine Leroux

Version of Record: https://www.sciencedirect.com/science/article/pii/S0022459621000268
Manuscript_1fcc588535f5ff8abe89541edb6a89fa

New cation deficient scheelites $(Sr,Ce)_nWO_4$ (n<1) : structural and optical properties

Andarair Gomes dos Santos[1,2], Madjid Arab[2], Carlson Pereira de Souza[3] and Christine Leroux[2]

[1] *Universidade Federal Rural do Semi-Árido, CCEN, Campus Mossoró-F. Mota, Costa e Silva, 59.625-900, Mossoró/RN, Brasil; email: andarair@ufersa.edu.br*

[2] *Aix Marseille Univ, Univ Toulon, CNRS, IM2NP, Marseille, France email: madjid.arab@univ-tln.fr,* leroux@univ-tln.fr*

[3] *Universidade Federal do Rio Grande do Norte, Campus Universitário, L. Nova, 59072-970, Natal/RN, Brasil; email: carlson@ufrnet.br*

**Corresponding author*

Abstract

New cation deficient tetragonal scheelites, $(Sr,Ce)_nWO_4$ (n<1); were synthesized using the Ethylene-DiamineTetraacetic Acid -citrate method. The chemical compositions and homogeneity of the powders were determined by Energy Dispersive Spectroscopy. Whatever the cerium amount, the cation deficient scheelites exhibit (3+2)D tetragonal incommensurate modulations, which evolve with increasing cerium and structural cations vacancies amount. The optical absorption onset varies from 400 nm to 450 nm with the increase of the Ce amount. The optical bandgap of the strontium cerium tungstates cation deficient scheelites (3.18 – 3.42eV) is much lower than the one of pure scheelite $SrWO_4$ (4.51eV) and near the one of $Ce_2W_3O_{12}$ (3.14 eV).

Keywords: cation deficient scheelite; incommensurate modulations; strontium cerium tungstate; optical bandgap; transmission electron microscopy.

Introduction

Scheelite tungstates and molybdates are nowadays widely studied because of their tuneable optical properties, associated to excellent thermal and chemical stability [1-6]. In particular, when doped with rare earths, they were valued to be high potential materials for White Light Emitting Diode (WLED) , as multicolor light emitters [7,8], red emitters [9 ,10]. They proved also to possess interesting catalytic properties for the production of H_2 [11-13]. Undoped tetragonal scheelite ABO_4 were found to have extra

low thermal conductivity [14], and have been also investigated as photoanodes [15], photocatalysts [16] or for nuclear waste immobilization [17].

The general formula of tetragonal scheelite is ABO_4, with a huge variety of cations on the A sites, and B being mainly occupied by W, Mo, but also V [18, 19]. The scheelite structure can accommodate various cations substitutions on the A site, allowing a tuning of the properties. The substitution by rare earth cations RE on the A sites modifies several properties of the scheelite compounds, such as promoting ionic conduction, so reducing the width of the forbidden band andchanging the spectral range of the visible light absorption and of the photoluminescence emissions [10,20-21].

Substituted scheelite related compounds with a tetragonal structure can be written $(A, A')_n[(B, B')O_4]$ ($n \leq 1$) [3], with $n<1$ implying vacancies on the A site, leading to so called cation deficient scheelites [1-2,22]. With a rare earth ion RE^{3+} as substituting cation, the scheelites can be non deficient (n=1) if A sites are occupied by an alkali ion with a 1^+ charge [1,23-24] and deficient if A sites are occupied by a cation 2^+ (this work) [18,25-26]. Amongst them, scheelite structures with Ce^{3+} as RE^{3+} are seldom [27-28] because of the relativity instability of this cation in air which can lead to the formation of CeO_2 [29].

In cation deficient scheelites, the cations and the structural vacancies on the A site can be more or less ordered, and incommensurate superstructures can appear [22,27]. The appearance of incommensurate modulations is directly linked to the amount of structural vacancies. Batuk et al. [21] showed that for $Ca_{0.85-1.5x}Gd_xEu_{0.1\ \ 0.05-0.5x}WO_4$ ($0<x<0.567$), at low vacancies concentrations ($x\leq0.15$) cations and cations vacancies are randomly distributed, as for higher vacancy concentrations ($0.2\leq x<0.33$), the scheelite structure evolves from a incommensurate structure (3+2)D tetragonal symmetry to a monoclinic distortion with a (3+1)D superstructure and a monoclinic phase $A_2(BO_4)_3$.

Previously, a new deficient tetragonal scheelite with a high amount of cerium (35%) was synthesized [27], and the catalytic properties of this phase for the partial oxidation of methane and production of H_2 was investigated [12]. The aim of the present work was to synthezise tetragonal strontium cerium scheelites compounds with various cerium contents (from 20% to 50%) in order to study the influence of cerium and structural vacancies on the structure and optical properties of the compounds. The exact chemical composition of the powders was determined by Energy Dispersive Spectroscopy (EDS). To the best of our knowledge, chemical compositions and chemical homogeneity are not often measured in substituted scheelites and a solid

solution with nominal composition is generally assumed. A somewhat similar attempt of synthesis of cerium substituted strontium molybdates with nominal composition $Sr_{1-x}Ce_xMoO_4$ (x=0.1, 0.2, 0.3, 0.4, 0.5) has been recently published [28]. However, no experimental proof is given in the paper of the real composition and of the homogeneity of the obtained powders. In this work, the structural characterization was performed by X rays diffraction, transmission electron microscopy and electron diffraction. The optical band gap and absorption onsets were determined by UV–Visible diffuse reflectance spectroscopy.

Experimental procedure

Chemical products

Strontium nitrate, cerium nitrate precursors, tungsten trioxide, citric acid, and Ethylene-DiamineTetraacetic Acid (EDTA) with a high purification level of 99 % were purchased from Sigma Aldrich. Ammonium hydroxide was obtained from Fluka. All the synthesis were carried out with 18 MΩ deionized water.

Synthesis of the $Sr_{0.75}Ce_{0.20}WO_4$, $Sr_{0.60}Ce_{0.30}WO_4$ and $Sr_{0.30}Ce_{0.50}WO_4$ via the EDTA-citrate method.

The different strontium cerium tungstates were synthesized via the EDTA-citrate method. This method is known to produce submicronic oxide powders. Binary tungstate such as $SrWO_4$ and $Ce_2W_3O_{12}$ as well as a tetragonal cation deficient scheelite compound $Sr_{0.5}Ce_{0.35}WO_4$ were already successfully obtained through this method [11, 12, 27, 30].

Strontium nitrate, cerium (III) nitrate hexahydrate and tungsten oxide were used as cations source. EDTA was diluted in ammonium hydroxide at 40°C with constant stirring for 15 min. Solutions 0.3M of strontium and cerium nitrates and WO_3 were added in the solution of the EDTA/NH_4OH in various proportions and stirred again for15 min. Then 0.45M citric acid was added to initiate the complexation reaction at a temperature of 80°C and at a pH of 9.0. The reaction time lasted 180 min until the appearance of a gel-like precipitate. This gel was subjected to a heat pretreatment in air at a temperature of 230°C for 180 min to remove waste liquids and volatiles, leading to the formation of a black powder with organic molecules still present in the powder. The final annealing was performed at 1000°C for 300 min in air, a temperature ensuring the crystallization of the gel, leading to yellowish white powders. The initial proportion of

strontium and cerium precursors was calculated insuring global charge neutrality and then adapted using the results of Electron Dispersive Spectroscopy (EDS) analysis until a single phased homogeneous powder was obtained.

Structural and chemical characterization

Transmission electron microscopy (TEM) and Electron Diffraction (ED) characterization were performed with a conventional Tecnai 200kV microscope equipped with a LaB_6 source. The chemical composition of the ternary tungstate in strontium, cerium and tungsten was determined by Electron Dispersive Spectroscopy (EDS). The quantification of cation concentrations was realized using standards. The binary compounds $SrWO_4$ [11,12] and $Ce_2W_3O_{12}$ [30] were used as standards for the determination of the $K_{Sr/W}$ and $K_{Ce/W}$ factors. The statistical study of chemical homogeneity of the powder consisted in 25 analyses on randomly chosen grains.
X-ray powder diffraction (XRD) patterns were collected in the classical θ-2θ mode, from 10° to 80° (step size 0.003°, scan speed 0.004°s^{-1}), with an Empyrean Panalytical diffractometer, equipped with a Cu anti-cathode. The XRD patterns were refined using the software Material Analysis Using Diffraction MAUD version 2.064 [31]. Starting from data CIF files found in literature (ICSD), cell parameters and atomic positions were obtained [32]. The background was fitted with a 5 th order polynomial function and the peaks with pseudo-Voigt functions. Bond lengths and bond angles were calculated from the refined results using Crystal Maker.

Optical properties

The UV–Visible diffuse reflectance spectra (DRS) of different samples were recorded using a Shimadzu 2600 UV/Vis spectrophotometer along with a 150 mm integrating sphere and using $BaSO_4$ as the baseline reference. The measurements were performed in the range of 250–800 nm at room temperature with a resolution of 0.08nm. The background was determined using a calibrated reflectance standard to obtain a reflectance accuracy of 0.005.

Results and Discussion

Structural, morphological characterization and composition analysis

The nominal composition of the powders with respectively, 0.2, 0.3, 0.4, 0.5 Ce was first calculated using charge neutrality of the compounds, assuming a charge 2^- for $[WO_4]$, as it is the case for the $SrWO_4$ scheelite structure. The corresponding theoretical compositions are then $Sr_{0.70}Ce_{0.20}WO_4$, $Sr_{0.55}Ce_{0.30}WO_4$, $Sr_{0.40}Ce_{0.40}WO_4$ and $Sr_{0.25}Ce_{0.50}WO_4$. EDS analysis showed that the obtained powders were inhomogeneous in composition. Thus, the composition was optimized until homogeneous single phased powders were obtained. Fig.1 shows the spectra obtained on the homogeneous powders, and Table 1 shows the mean values of strontium and cerium composition of the powders. The attempts to synthesise a powders with 40% Ce led to two phased powders.

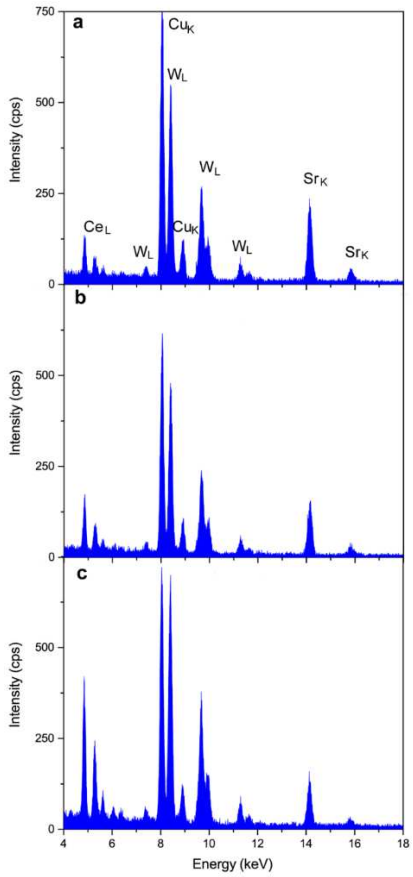

Figure 1. EDS spectra of (a) $Sr_{0.75}Ce_{0.20}WO_4$, (b) $Sr_{0.60}Ce_{0.30}WO_4$ and (c) $Sr_{0.30}Ce_{0.50}WO_4$ obtained via the EDTA-citrate method.

Table 1. Chemical composition of single phased $(Sr,Ce)_nWO_4$ powders.

Sample	Sr mean value	Ce mean value	Standard

			deviation
$Sr_{0.3}Ce_{0.5}WO_4$	0.33	0.47	0.04
$Sr_{0.5}Ce_{0.35}WO_4$ [23]	0.50	0.35	0.03
$Sr_{0.6}Ce_{0.3}WO_4$	0.60	0.29	0.03
$Sr_{0.75}Ce_{0.2}WO_4$	0.75	0.19	0.05

The single phased scheelites are all cation deficient. The structural cation vacancies amount on the (Sr,Ce) sites varies by a step of 0.05, from 0.05 for $Sr_{0.75}Ce_{0.20}\ _{0.05}WO_4$, to 0.20 for $Sr_{0.30}Ce_{0.50}\ _{0.2}WO_4$. This latter amount of structural cation vacancies is near the highest amount of vacancies already observed in the case of deficient scheelites where the 2^+ cation is partially substituted by RE $^{3+}$. For $Cd_{1-3x}\ _xRE_{2x}\ MoO_4$ the maximum of vacancies is 0.25 [33] as for $Pb_{1-3x}\ _xRE_{2x}\ Eu_{2x}\ (MoO_4)_{1-3x}(WO_4)_{3x}$ the maximum of vacancies is near 0.2 [34]. The obtained compositions in strontium and cerium correspond to a +2.1 cation charge that should be compensated to ensure global charge neutrality. Assuming W is in a 6+ state, interstitial oxygen ions will compensate the excess of positive charge. Indeed, scheelite compounds, due to their structure, easily accommodate interstitial oxygens [20, 35-36]**.** Concerning the morphology of the obtained powders (Fig. 2), the EDTA complexation method led to well crystallized grains with a high inhomogeneous size distribution

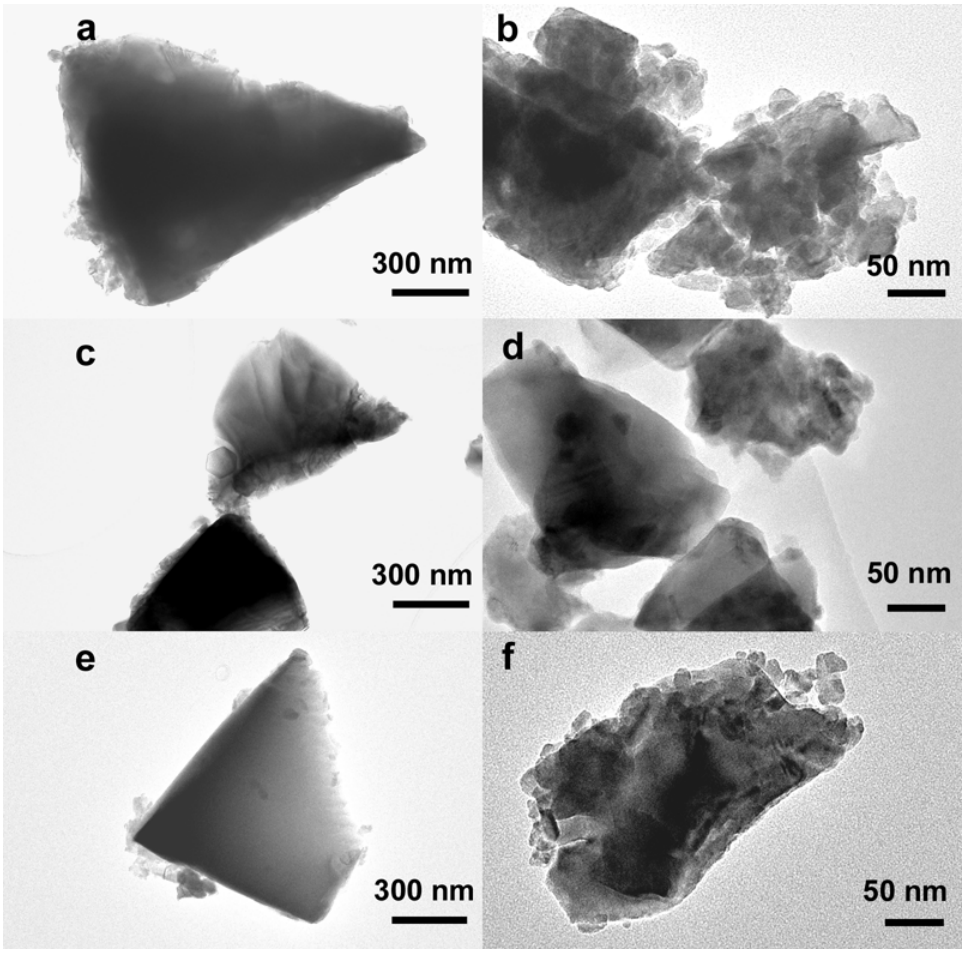

Figure 2. TEM images showing the two grain types observed in the different powders $Sr_{0.75}Ce_{0.20}WO_4$ (a, b), $Sr_{0.60}Ce_{0.30}WO_4$ (c, d) and $Sr_{0.30}Ce_{0.50}WO_4$ (e, f). Each powder contains sub micronic (a, c, e), and nanometer (b, d, f) grains.

In each powder , one can find monocrystalline submicronic grains (Fig.2.a, c, e), but also grains in the nanometer range as small as 20-30 nm (Fig.2.b, d, f). This inhomogeneity of the grains size is specific of the EDTA-citrate method [11,27]. Whatever the amount of cerium, no particular morphology can be observed, although the submicron grains are platelet-like. Again, this morphology of submicronic monocrystalline grains is characteristic of the tetragonal scheelite tungstate obtained by this synthesis method.

The previous structural study about $Sr_{0.50}Ce_{0.35}WO_4$ [27] showed that this strontium cerium tungstate adopts a tetragonal structure with the space group $I\bar{4}$ (n°82), thus a reduced symmetry with regards to the usual $I4_1/a$ scheelite space group. This symmetry loss leads to a splitting of atomic positions, as can be seen in Table 2.

Table 2. Coordinates of Sr, Ce, W and O in $I4_1/a$ and $\bar{I}4$ space groups

Space group	Atom	Site	Coordinates
$I4_1/a$	Sr, Ce	4b	0,0,1/2 0,1/2,3/4
	W	4a	0,0,0 0,1/2,1/4
	O	16f	x,y,z
$\bar{I}4$	Sr, Ce	2b	0,0,1/2
	Sr, Ce	2c	0,1/2,1/4
	W	2a	0,0,0
	W	2d	0,1/2,3/4
	O_1 O_2	8 g	x,y,z

Furthermore, a two dimensional incommensurate modulation was evidenced, with the two incommensurate vectors, **q_1=0.54 a*+0.82 b*, q_2=-0.82 a*+0.54 b*,** which led to an indexation of the different ED patterns in the (3+2)D superspace group as $\bar{I}4\,(\alpha,\beta,0,-\beta\alpha 0)00$, with α=0.54 and β=0.82 [37]. In this work, the same incommensurate vectors are observed **q_1, q_2** for the various powders. Fig.3 shows ED patterns with a [001] zone axis of $Sr_{0.75}Ce_{0.20}WO_4$ $Sr_{0.60}Ce_{0.30}WO_4$ and $Sr_{0.30}Ce_{0.50}WO_4$ indexed in the same superspace group. The intensity of the incommensurate modulations varies with the amount of cerium, hence with the amount of structural cation vacancies. The ED pattern of $Sr_{0.75}Ce_{0.20}{}_{0.05}WO_4$ exhibits very faint incommensurate modulations (Fig.3a), while for $Sr_{0.60}Ce_{0.30}{}_{0.1}WO_4$ (Fig.3b) and $Sr_{0.30}Ce_{0.50}{}_{0.2}WO_4$ (Fig.3c), ED patterns show incommensurate spots with increasing intensities. A variation of the incommensurate modulations with (3+2)D tetragonal symmetry was already observed in $Ca(Gd,Eu)WO_4$ compounds [21], with no incommensurate modulations for cations vacancy concentrations less than 0.15 and for higher vacancies concentrations (0.2) incommensurate (3+2)D modulations were observed. For 0.33 concentration, the modulations changed to a monoclinic 1 D symmetry. Our results agree with those of [21] for high structural vacancy concentration of 0.15 and 0.2, but contrary to [21] the modulations (3+2)D appears in strontium cerium tungstate at very low vacancy concentrations (0.05).

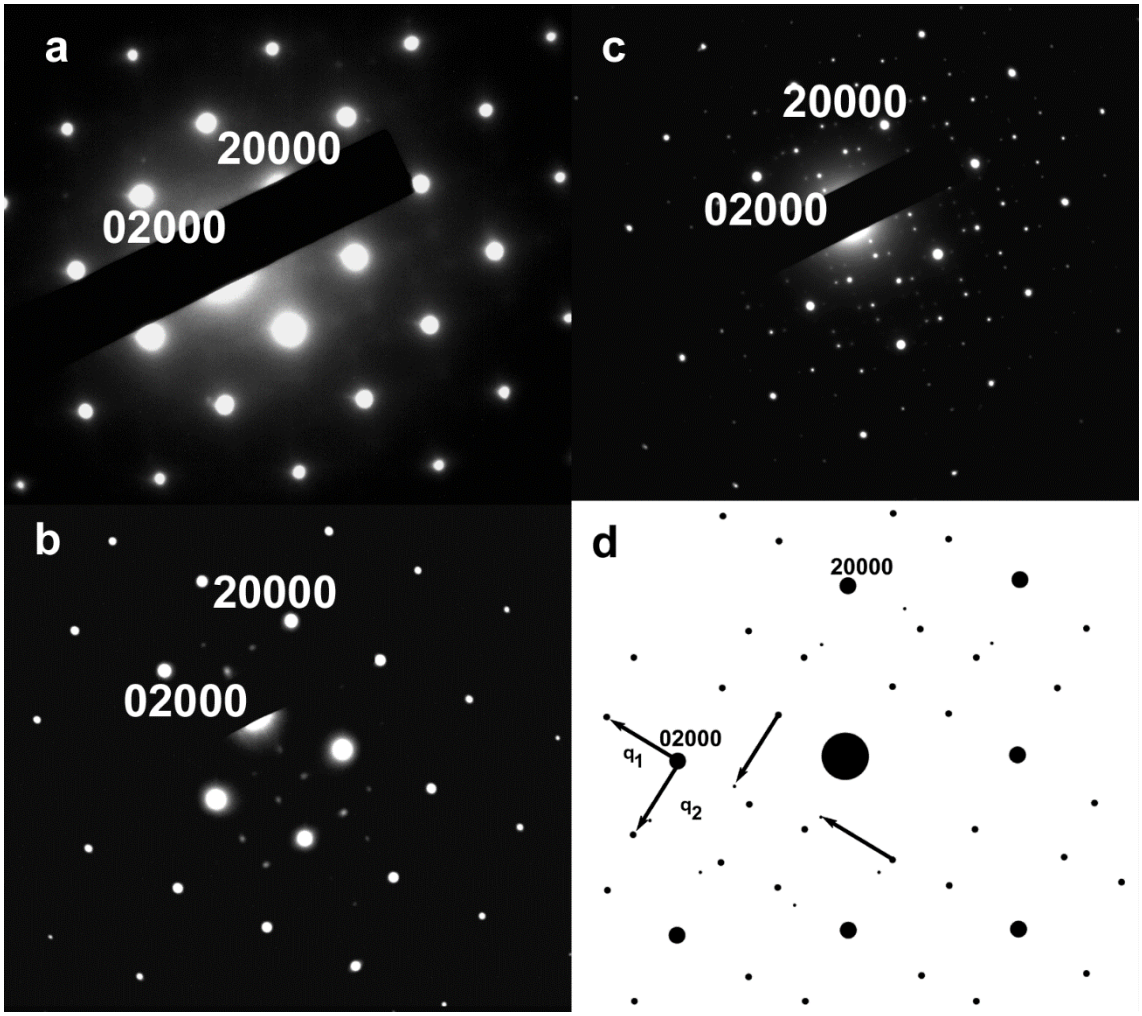

Figure 3. Electron diffraction pattern in the [001] zone axis of $Sr_{0.75}Ce_{0.20}WO_4$ (a), $Sr_{0.60}Ce_{0.30}WO_4$ (b) and $Sr_{0.30}Ce_{0.50}WO_4$ (c). (d) is a drawing of the [001] ED showing the supplementary spots due to $\mathbf{q_1}$ and $\mathbf{q_2}$ incommensurate modulation vectors.

Powder X-ray diffraction and Rietveld refinements

The X-ray diffraction patterns of $Sr_{0.75}Ce_{0.20}WO_4$, $Sr_{0.60}Ce_{0.30}WO_4$ and $Sr_{0.30}Ce_{0.50}WO_4$ powders are shown Fig.4. The patterns of the different powders calcined at 1000°C show the diffraction peaks of the tetragonal scheelite phase (43219-ICSD), even for a high amount of cerium (50%). Let us recall that the pure cerium scheelite compound $Ce_2W_3O_{12}$ is a monoclinic distorted scheelite [30]. The structural parameters were obtained from the Rietveld refinement method using the MAUD software, in the $I\bar{4}$ space group, with a cif file already published [25]. In this space group, cations are in fixed positions, so only oxygen positions were refined. The A sites were randomly occupied by Ce^{3+} and Sr^{2+} in the proportion corresponding to each chemical composition obtained.

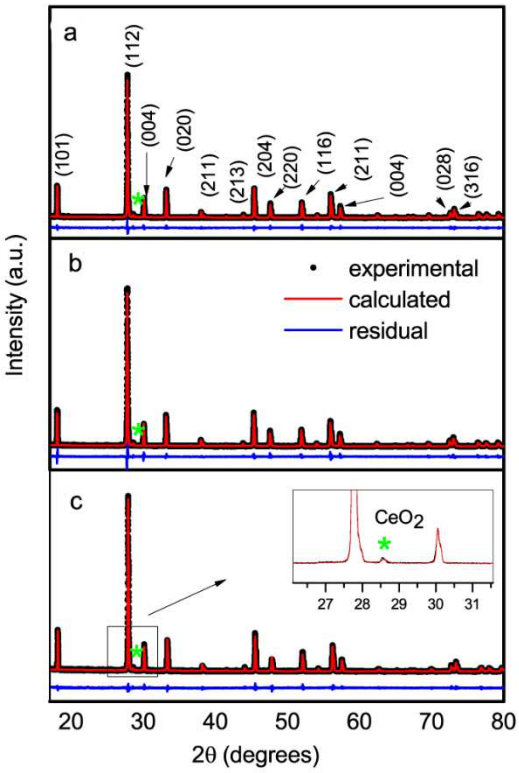

Figure 4. XRD patterns of powders (a) $Sr_{0.75}Ce_{0.20}WO_4$, (b) $Sr_{0.60}Ce_{0.30}WO_4$ and (c) $Sr_{0.30}Ce_{0.50}WO_4$ obtained via the EDTA-citrate method.

The solid black line in Fig.4 represents the experimental points, the red line corresponds to the XRD pattern calculated from the Rietveld refinement method and the blue line (residual) the difference between the experimental data and the calculated data. The refined cell parameters, oxygen coordinates and reliability factors are reported in Table 3. The cell parameters error is 2.10^{-4} and the error on oxygen positions is 2.10^{-3}.

A small diffraction peak, indicated by a star (*) in Fig.4, could be attributed to the CeO_2 phase (72155-ICSD). All Rietveld refinements were done assuming the presence of CeO_2

and the weight % of this residual phase was found to be 2%. The presence of a CeO_2 phase was also observed in the synthesis of cerium molybdate at temperatures above 600°C [38]. The presence of CeO_2 is due to the relatively high instability of the trivalent Ce ion [29], leading to its oxidation. The kinetic of this oxidation is related to the high concentration of oxygen in the medium, due to the agitation, as well as the pH, favoring

precipitation of the cerium 4+ in the oxide form [39]. We optimized the synthesis parameters so that the amount of CeO_2 phase remained less than 2% in the powders.

Table 3. Refinement results for the ternary $Sr_{0.75}Ce_{0.20}WO_4$ $Sr_{0.60}Ce_{0.30}WO_4$ and $Sr_{0.50}Ce_{0.30}WO_4$ compounds in the $I\bar{4}$ space group.

Compound	$Sr_{0.75}Ce_{0.20}WO_4$	$Sr_{0.60}Ce_{0.30}WO_4$	$Sr_{0.30}Ce_{0.50}WO_4$
Space group	$I\bar{4}$	$I\bar{4}$	$I\bar{4}$
Cell parameters (Å)	a=5.4055 c=11.9049	a=5.3977 c=11.8792	a=5.3762 c=11.8708
Cell volume ($Å^3$)	347.859	346.099	343.112
Oxygen coordinates (8g)	O_1 / O_2	O_1 / O_2	O_1 / O_2
X	0.248	0.246	0.226
	0.656	0.648	0.673
Y	0.129	0.133	0.127
	0.806	0.804	0.789
Z	0.933	0.931	0.932
	0.152	0.156	0.148
Reliability factors			
R_{wp}	10.0	10.2	11.1
R_{exp}	7.7	8.1	8.8
R_{wp}/R_{exp}	1.31	1.26	1.27

The variations with the cerium content of the cell parameters, as well as the cell volume and c/a ratio are drawn in Fig.5.

The cell parameters decrease with the increasing of cerium content. This was expected since Ce^{3+} has a smaller radius than Sr^{2+} (Δr=-12 pm) and the increase of Ce^{3+} amount induces an increase of the structural vacancies amount.

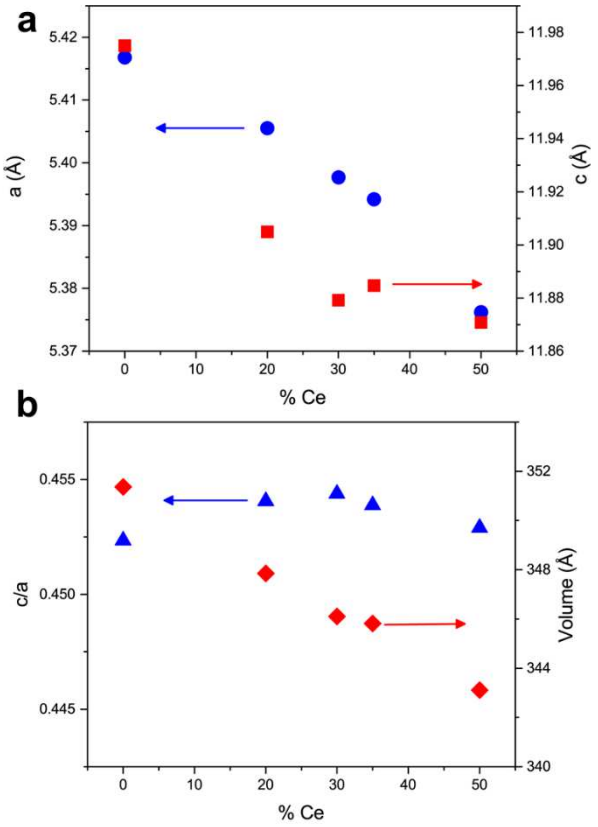

Figure 5. a) Cell parameters variations with the cerium amount in the tetragonal scheelite compound. b) Cell volume and c/a ratio variations with the cerium amount. The values for $SrWO_4$ and $Sr_{0.5}Ce_{0.35}WO_4$ were already published [23].

The a cell parameter varies continuously, but one can notice a change in the variation of the c cell parameter around 30% Ce, with a decrease of c between 0 and 30% , and almost no variation between 30 and 50% Ce (Fig.5a). The c/a ratio is the highest for 30% of cerium (Fig.5b). Let us recall that the ABO_4 tetragonal scheelite can be described as the piling up along the c axis of layers of isolated WO_4 tetahedra separated by AO_8 polyhedra. The presence of structural vacancies tend to shrink the piling up, as can be seen in $Ce_2W_3O_{12}$ [30], which correspond to a monoclinic deformed scheelite structure with one layer over 3 without AO_8 polyhedra. The cell volume decreases continuously with the cerium content, as was expected considering the ionic radii of Ce^{3+} and Sr^{2+},with a total volume variation of 2.5 % between 0 and 50% Ce. The different refined oxygen positions, presented Table 3, led to different bond lengths and bond angles of the WO_4 and AO_8 (A=Sr,Ce) polyhedra. These were calculated using the Crystal Maker software and are gathered in Table 4. In $SrWO_4$, the WO_4 tetrahedra are regular, with a bond length of 1.841Å [27]. In the $I\bar{4}$ space group, there are two WO_4 tetrahedra. The two W-O bond lengths for $Sr_{0.75}Ce_{0.20}WO_4$,

$Sr_{0.60}Ce_{0.30}WO_4$ and $Sr_{0.30}Ce_{0.50}WO_4$ increasingly deviate from this value with cerium content. For low cerium content, both bonds are shorter, corresponding to a contraction of the tetrahedra, as for high cerium content (50%) one tetrahedra is even more contracted but the other one is expanded. The W-O bond lengths in $Sr_{0.30}Ce_{0.50}WO_4$ are close to those obtained in $Ce_2W_3O_{12}$, the pure cerium tungstate [30]. Thus, the variation of W-O bond lengths and the increasing distortion of the tetrahedra with the increase of cerium are coherent. The bond angles O-W-O do not change significantly with the amount of cerium. The AO_8 polyhedra in the $Sr_{0.75}Ce_{0.20}WO_4$, $Sr_{0.60}Ce_{0.30}WO_4$ and $Sr_{0.30}Ce_{0.50}WO_4$ structures are expanded compared to those in $SrWO_4$ and the deviations of the bond lengths increase with the cerium content.

Table 4. Bond lengths and bond angles in [WO_4] and [AO_8] polyhedra for the $Sr_{0.75}Ce_{0.20}WO_4$, $Sr_{0.60}Ce_{0.30}WO_4$ and $Sr_{0.30}Ce_{0.50}WO_4$ compounds.

Compound		$Sr_{0.75}Ce_{0.20}WO_4$	$Sr_{0.60}Ce_{0.30}WO_4$	$Sr_{0.30}Ce_{0.50}WO_4$
Polyhedra			*WO_4*	
Bond (Å)	W(2a)-O_1	1.705	1.715	1.616
	W(2d)-O_2	1.778	1.734	1.903
Angle (º)	O_1-W(2a)- O_1	102.5	103.1	104.6
		124.6	123.1	119.7
	O_2-W(2d)- O_2	98.2	100.1	100.7
		115.4	114.3	114.0
			AO_8	
Bond (Å)	A(2b)- O_1	2.551	2.546	2.615
	A(2b)- O_2	2.595	2.602	2.525
	A (2c)- O_1	2.667	2.651	2.670
	A (2c)- O_2	2.749	2.742	2.643
Angle (º)	O-A(2b)-O	62.7	64.7	62.3
		72.4	70.8	73.7
		82.4	82.5	81.3
		91.5	88.9	92.0
		95.5	95.9	95.5
		119.1	120.6	118.8
		143.8	142.5	143.8
		153.1	152.3	153.7

Angle (º)	O-A(2c)-O	61.4	63.2	58.7
		70.1	71.4	73.9
		77.5	78.0	77.6
		81.0	79.1	81.7
		100.3	99.5	102.2
		129.9	131.2	125.3
		132.1	132.1	129.6
		148.2	148.1	151.5

Optical properties

The optical properties of the cation deficient scheelite compounds were obtained by UV – Vis diffuse reflectance at room temperature. In Fig.6, the optical absorption spectra of the $Sr_{0.75}Ce_{0.20}WO_4$, $Sr_{0.60}Ce_{0.30}WO_4$ and $Sr_{0.30}Ce_{0.50}WO_4$ powders show absorption onsets associated to the electronic transitions in the wavelength range from 405 to 470 nm. This confirms an absorption in the blue light region of the visible spectra for these scheelites, with a shift towards higher wavelengths for increasing Ce amount. Basically, the absorption behavior in AWO_4 (such as A= Ca, Sr, Pb) only depends only on the transition between O2p oxygen states of the valence band (VB) and the W4f -5d tungsten states of the conduction band (CB) [40]. Furthermore, the Sr orbitals do not appear in the forbidden band gap.

The redshift of the absorption spectra with Ce insertion is due to the appearance of new energy levels in the band gap, which can be induced by crystal defects, structural distortion andimpurities [41-42].

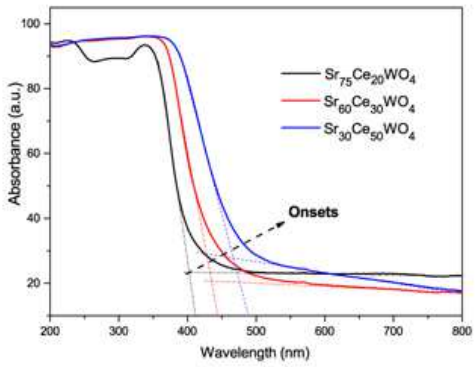

Figure 6. Absorbance of the powders $Sr_{0.75}Ce_{0.20}WO_4$,$Sr_{0.60}Ce_{0.30}WO_4$ and $Sr_{0.30}Ce_{0.50}WO_4$ obtained via the EDTA-citrate method.

The optical bandgap energy (E_g) values were deduced from the Kubelka – Munk equation. The Kubelka – Munk function $F(R_\infty)$ for any wavelength is described by $F(R_\infty) = {K}/{S} = {(1-R_\infty)^2}/{2R_\infty}$, where R_∞ designates the absolute reflectance of the sample at infinite thickness [43] . K represents the molar absorption coefficient and S is the scattering coefficient. The optical bandgap can be deduced by the following equation 1 [44-47]:

$$\alpha h\nu = A\left(h\nu - E_g\right)^{n/2} \quad (1)$$

where α is absorption coefficient, hν corresponds to the incident photoenergy, A is a constant linked to the material andhe index n corresponds to the electronic transition characteristic of the used semiconductor. For the deficient scheelite structure ($Sr_{0.75}Ce_{0.20}WO_4$, $Sr_{0.60}Ce_{0.30}WO_4$ and $Sr_{0.30}Ce_{0.50}WO_4$) the electronic transitions were based on the direct bandgap, so n=1 [48] . The bandgap energy of the obtained materials can be evaluated by extrapolating the linear part of the $(F(R) * E)^2$ as a function of E=*hν* energy. As shown in Fig.7, the deduced bandgap energies are respectively 3.42, 3.31 and 3.18 eV for samples with 20, 30 and 50% of Ce content.

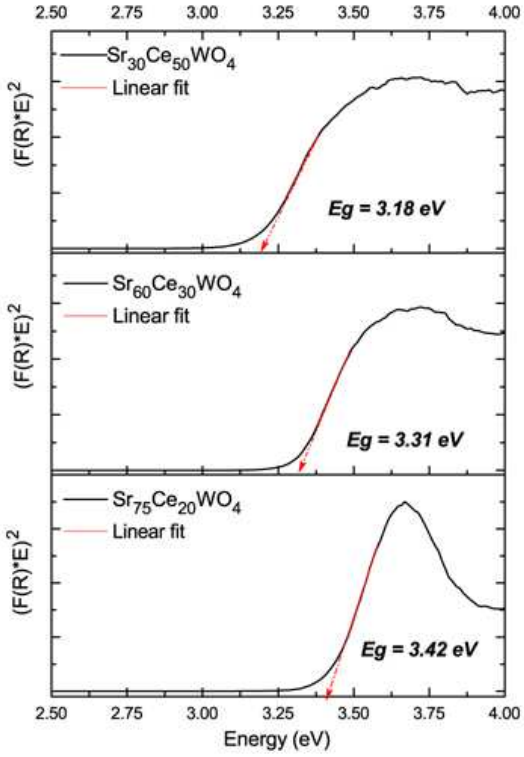

Figure 7. UV–vis absorbance spectra at room temperature of $Sr_{0.75}Ce_{0.20}WO_4$, $Sr_{0.60}Ce_{0.30}WO_4$ and $Sr_{0.30}Ce_{0.50}WO_4$ powders.

These values are much lower than that of pure $SrWO_4$ (4.51eV), but near the one of $Ce_2W_3O_{12}$ (3.14 eV) [27]. The band gap energies of the cation deficient $(Sr,Ce)_nWO_4$ (n<1) scheelites are in the same order of the calculated bandgap of polyoxometalate cluster $[Ce(W_5O_{18})^2]^{8-}$ [49], for which the electron density consists on the O2p atomic orbital for the HOMO and the Ce 4f orbitals for the LUMO.

As reported in literature, the band gap edge energies depend on the degree of structural order – disorder in the lattice [42] . They are also influenced by the synthesis methodology, pH of the precursor, and the size and morphology of the grains [41]. However, for the different $(Sr,Ce)_nWO_4$ scheelites, no difference in size and morphology could be evidenced, and the synthesis method was the same, soo, the energy band gap change can only be attributed to the presence of cerium and to the induced structural distortions.

The detailed analysis of the obtained microstructural data shows a strong distortion modification as the Ce quantity increases, hence the structural cation vacancies. The WO_4 polyhedra retracts with the decrease of the W–O bond length and AO_8 expands with the increase of the A–O bond length (see Table 4). Fig.8 shows the link between bandgap energy and cation concentration.

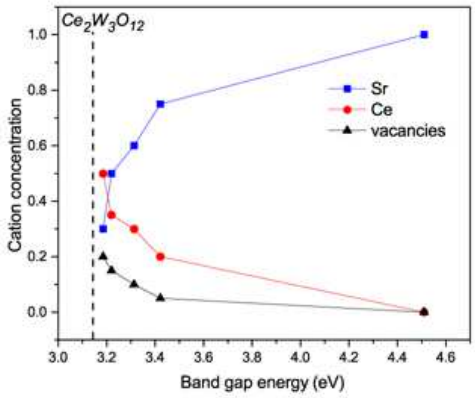

Figure 8. Cation vacancies and cations amount versus bandgap energy (eV)

The energy values are around 3.2-3.4 eV, thus are very different from the energy bandgap value of tetragonal $SrWO_4$.

The lower limit for strontium cerium tungstates bandgap energies corresponds to the bandgap of $Ce_2W_3O_{12}$ [27, 50]. As reported in litterature, the band gap energy of the AWO_4 scheelite materials was estimated to be greater than 4 eV [48]. Apart from band structure studies on normal and deformed AWO_4 scheelite structures, no theoretical band structure studies have been reported in the literature on deficient strontium cerium tungstates. To understand the influence of Ce on the band structure, one can consider the monoclinic deformed scheelite structure of $Ce_2W_3O_{12}$. In this compound, the Ce 4f orbital (juste below the Fermi level) lies between the O2p bonding orbitals and the W 5d antibonding orbitals, indicating that the Ce 4f orbital does not hybridize with W and/or O [50]. The Ce 4f orbital works as donor orbital. In addition, distorsions and defects significantly modify the electronic properties and the optical band gap of the compounds. The presence of defects, cations vacancies and ordering of A cations and vacancies can be a new parameter in controlling the scheelite structure and the related properties [22, 25-26, 51-52]. Several studies reported that the deformation of WO_4 tetrahedra lead to a reduction in the bandgap width [40, 48, 51, 53]. The disorder in $SrWO_4$ associated to the structural relaxation, leads to the presence of additional electronic levels in the bandgap [52, 54]. In this case, the localized levels O2p loose the bond with the tungsten for states appearing above the VB and W $5dz^2$ for states appearing below the CB [26,52,54].

Conclusion

New cation deficient modulated strontium cerium tungstates with the tetragonal scheelite structure were obtained via the EDTA-citrate method. Only specific compositions could be obtained, with structural cations vacancies on the A site varying by step of 0.05, from 0.05 for $Sr_{0.75}Ce_{0.20}WO_4$, to 0.20 for $Sr_{0.30}Ce_{0.50}WO_4$.The charge compensation may be ensured by interstitial oxygens. The cation deficient scheelites exhibit incommensurate modulations, whose intensities vary with the amount of cerium, thus with the amount of cation vacancies. The associated optical absorption occurs in the visible region between 400 nm and 470 nm and Ce insertion induces a redshift of

the absorption spectra edges. The electronic transitions were based on an direct bandgap semiconductor, with bandgap energies of 3.42eV ($Sr_{0.75}Ce_{0.20}WO_4$), 3.31eV ($Sr_{0.60}Ce_{0.30}WO_4$) and 3.18 eV ($Sr_{0.30}Ce_{0.50}WO_4$).The tetragonal structure of the strontium cerium tungstates exibits increasing polyhedra distorsions with increasing amount of cerium. Theoretical investigations are needed to take into account the defects present in the structure and the role of Ce on the band structure of these compounds.

Acknowledgement

One of the author thanks UFERSA and CAPES (Brazil) for financial support.

REFERENCES

[1] J. Huang, J. Xu, H. Luo, X. Yu, Y. Li, Effect of alkali-metal ions on the local structure and luminescence for double tungstate compounds, $AEu(WO4)_2$ (A = Li, Na, K),Inorg. Chem., 50, 11487–92, 2011.

[2] V. A. Morozov, D. Batuk , M. Batuk , O. M. Basovich ,E.G. Khaikina , D.V. Deyneko, B. I. Lazoryak, I. I. Leonidov, A. M. Abakumov, and J. Hadermann, Luminescence property upgrading via the structure and cation changing in $Ag_xEu_{(2-x)/3}WO_4$ and $Ag_xGd_{(2-x)/3-0.3}Eu_{0.3}WO_4$, Chem. Mat., 29, 8811-8823, 2017.

[3] V. Morozov, D. Deyneko, O. Basovich, E. G. Khaikina, D. Spassky, A. Morozov, V. Chernyshev, A. Abakumov, and J. Hadermann, Incommensurately modulated structures and luminescence properties of the $Ag_xSm_{(2-x)/3}WO_4$ (x=0.286, 0.2) scheelites as thermographic phosphors, Chem. Mat., 30, 4788–4798, 2018.

[4] J. Ruiz-Fuertes, A. Friedrich, D. Errandonea, A. Segura, W. Morgenroth, P. Rodríguez-Hernández, A. Muñoz, and Y. Meng, Optical and structural study of the pressure-induced phase transition of $CdWO_4$, Phys. Rev. B 95, 174105, 2017.

[5] V. Monteseguro, J. Ruiz-Fuertes, J. Contreras-García, P. Rodríguez-Hernández, A. Muñoz and D. Errandonea, High pressure theoretical and experimental analysis of the bandgap of $BaMoO_4$, $PbMoO_4$, and $CdMoO_4$, Appl. Phys. Lett. 115, 012102, 2019.

[6] K. W. Meert, V. A. Morozov, A. M. Abakumov, J. Hadermann, D. Poelman, and P. F. Smet, Energy transfer in Eu3+ doped scheelites: use as thermographic phosphor, Optics Express 22, A961-A972, 2014.

[**7**] Z. Xia, W. Zhou, H. Du, J. Sun, Synthesis and spectral analysis of Yb3+/Tm3+/Ho3+-doped $Na_{0.5}Gd_{0.5}WO_4$ phosphor to achieve white upconversion luminescence, Mater.Res. Bull. 45, 1199–1202, 2010

[8] P. Jena, S. K. Gupta, V. Natarajan, O. Padmaraj, N. Satyanarayana, M. Venkateswarlu, On the photo-luminescence properties of sol–gel derived undoped and Dy3+ ion doped nanocrystalline Scheelite type $AMoO_4$ (A = Ca, Sr and Ba), Mater.Res. Bull. 64, 223–232, 2015

[9] W. Zhang, J. Long, A. Fan, J. Li, Effect of replacement of Ca by Ln (Ln = Y, Gd) on the structural and luminescence properties of $CaWO_4:Eu^{3+}$ red phosphors prepared via co-precipitation, Mater. Res. Bull 47, 3479–3483, 2012

[10] Q. Ning, C. Zhou, Y. Shi, Effect of Eu^{3+} doping on $ZnWO_4$ phosphors luminescent properties and study of J-O theory, J. Solid State Chem. 290, 121458 , 2020

[11] M. Arab, A. L. Lopes-Moriyama, T. R. Santos, C. P. Souza, J. R. Gavarri , Ch. Leroux, Strontium and cerium tungstate materials $SrWO_4$ and $Ce_2(WO_4)_3$: Methane oxidation and mixed conduction. Catal. Today 208, 35– 41, 2013.

[12] R. H. Damascena dos Passos, C. Pereira de Souza, Ch. Leroux, M. Arab, Catalytic properties of $Sr_{1-x}Ce_xWO_4$: the role of mixed conduction in methane oxidation. Int. J. Hydrog. Energy 43, 15918-15930, 2018.

[13] J. Yang , X. Sun , C. Zeng , Q. Deng , Y.Hu , T. Zeng , J. Shi , Effect of La-doped scheelite-type $SrWO_4$ for photocatalytic H_2 production, Ionics 25, 5083–5089, 2019.

[14] Y. Liu, D. Jia, Y. Zhou, Y.Zhou , J. Zhao , Q. Li , B. Liu , Discovery of ABO_4 scheelites with the extra low thermal conductivity through high-throughput calculations, Journal of Materiomics 6, 702-711, 2020

[15] S. Li, K. L. Bychkov, D. S. Butenko, K. V. Terebilenko, Y. Zhu, W. Han, V. N. Baumer, M. S. Slobodyanik, H. Ji and N. I. Klyui, Scheelite-related $M^{II}_xBi_{1-x}V_{1-x}Mo_xO_4$ (M^{II} – Ca, Sr) solid solution-based photoanodes for enhanced photoelectrochemical water oxidation, Dalton Trans. 49, 2345-2355, 2020

[16] C. Shivakumara, R. Saraf, S. Behera, N. Dhananjaya , H. Nagabhushana , Scheelite-type MWO_4 (M = Ca, Sr, and Ba) nanophosphors: Facile synthesis, structural characterization, photoluminescence, and photocatalytic properties, Mater. Res.Bull. 61, 422–432, 2015

[17] E. A. Potanina, A. I. Orlova, D. A. Mikhailov, A. V. Nokhrin, V. N. Chuvil'deev, M. S. Boldin, N. V. Sakharov, E. A. Lantcev, M. G. Tokarev, A. A. Murashov, Spark Plasma Sintering of fine-grained $SrWO_4$ and $NaNd(WO_4)_2$ tungstates ceramics with the scheelite structure for nuclear waste immobilization, J. Alloys Compd. 774, 182-190, 2019.

[18] B. Xiao and M. Schmidt, Incorporation of Europium (III) into scheelite-related host matrixes ABO_4 (A = Ca^{2+}, Sr^{2+}, Ba^{2+}; B = W^{6+}, Mo^{6+}): Role of A and B sites on the dopant site distribution and photoluminescence, Inorg. Chem. 56 14948−14959, 2017.

[19] A.W. Sleight, K.Ayan, D. B. Rogers, New nonstoichiometric molybdate, tungstate and vanadate catalysts with the scheelite type structure, J. Solid State Chem. 13, 231-236, 1975

[20] T. Esaka, Ionic conduction in substituted scheelite-type oxides, Solid State Ionics 136–137, 1–9, 2000

[21] D. Batuk, M. Batuk, V. A. Morozov, K. W. Meert, P. F. Smet, D. Poelman, A. M. Abakumov, J. Hadermann, Effect of cation vacancies on the crystal structure and luminescent properties of $Ca_{0.85-1.5x}Gd_xEu_{0.1\ \ 0.05-0.5x}WO_4$ ($0<x<0.567$) scheelite-based red phosphors, J. Alloys Compd. 706, 358-369, 2017.

[22] V. Morozov, A. Arakcheeva, B. Redkin, V. Sinitsyn, S. Khasanov, E. Kudrenko, M. Raskina, O. Lebedev, G. Van Tendeloo, $Na_{2/7}Gd_{4/7}MoO_4$: A modulated scheelite-type structure and conductivity properties, Inorg. Chem. 51, 5313-5324, 2012.

[23] B. S. Barros, A. C. Lima, Z. R. Silva, D. M. A. Melo, S. C. Jr Alves, Synthesis and photoluminescent behavior of Eu^{3+}-doped alkaline-earth tungstates, J. Phys. Chem. Solids 73, 635-640, 2012.

[24] A .K. Munirathnappa, J. C. Neuefeind, P. Yanda, A. Sundaresan, I. V. Kityk, K. Ozga, J. Jedryka, P. Poornesh, A. Rao and N. G. Sundaram, Average structure, local structure, photoluminescence, and NLO properties of scheelite type $NaCe(WO_4)_2$, Cryst. Growth Des.19, 6082−6091, 2019.

[25] A. M. Abakumov, V. A. Morozov, A. A. Tsirlin, J. Verbeeck, J. Hadermann, Cation ordering and flexibility of the BO_4^{2-} tetrahedra in incommensurately modulated $CaEu_2(BO_4)_4$ (B = Mo, W) scheelites, Inorg. Chem. 53, 9407–9415, 2014.

[26] P. Jiang , W. Gao , R. Cong , T. Yang , Structural investigation of the A-site vacancy in scheelites and the luminescence behavior of two continuous solid solutions $A_{1-1.5x}Eu_x\square_{0.5x}WO_4$ and $A_{0.64-0.5y}Eu_{0.24}Li_y\square_{0.12-0.5y}WO_4$ (A = Ca, Sr; □ = vacancy), Dalton Trans. 44, 6175-6183, 2015.

[27] R. H. Damascena dos Passos, M. Arab, C. Pereira de Souza, Ch. Leroux, $Sr_{1/2}Ce_{5/14}\square_{1/7}WO_4$; a new modulated ternary scheelite compound, Acta Cryst. B 73, 466-473, 2017.

[28] V. Elakkiya, S. Sumathi, Low-temperature synthesis of environment-friendly cool yellow pigment: Ce substituted $SrMoO_4$, Mater. Lett. 263, 127246-127249, 2020

[29] C. Y. You, C. Colon, F. Fernandez-Martínez, I. Andres-García, Synthesis and characterization of a Ce^{3+} trivalent scheelite-type double tungstate by solid state method, J. Alloys Compd 694, 345-353, 2017.

[30] R. H. Damascena dos Passos, C. Pereira de Souza, C. Bernard-Nicod , Ch. Leroux, M. Arab, $Ce_2(WO_4)_3$, a catalyst for methane oxidation. Ceram. Int. 46, 8021-8030, 2020.

[31] M. Ferrari, L. Lutterotti , Method for the simultaneous determination of anisotropic residual stresses and texture by x-ray diffraction, J. Appl. Phys. 76, 7246-7255, 1994.

[32] R. A. Young, The Rietveld Method, International Union of Crystallography (IUCr); Oxford University Press Inc.: New York, NY, USA,1995.

[33] M. Guzik, E. Tomaszewicz , Y. Guyot , J. Legendziewicz , G. Boulon , Eu^{3+} luminescence from different sites in a scheelite-type cadmium molybdate red phosphor with vacancies, J. Mater. Chem. C 3, 8582-8594, 2015.

[34] M. Piatkowska, E. Tomaszewicz, Structural, morphological and optical properties of new Eu-doped and vacancied lead molybdato-tungstates, J. Rare Earths 36, 635-641, 2018.

[35] R. J. Packer S. J. Skinner, Remarkable oxide ion conductivity observed at low temperatures in a complex superstructured oxide, Adv. Mater. 22, 1613–1616, 2010.

[36] J. Wang, L. Zhou, Y. Wang, J. Xu, X. Yang, X. Kuang, Molecular dynamic simulation of interstitial oxide ion migration in $Pb_{1-x}La_xWO_{4+x/2}$ scheelite, J. Solid State Chem. 268,16–21, 2018

[37] S. Van Smaalen , Incommensurate crystallography, Oxford University Press, 2007

[38] M.S. Sena, M.M.S. Silva, A.G. Santos, A.L. Lopes-Moriyama, C.P. Souza, Synthesis and characterization of cerium molybdate semiconductor nanoparticles, Mater. Res. 20, 485-491, 2017.

[39] J.F. Brazdil, Scheelite: a versatile structural template for selective alkene oxidation catalysts, Catal. Sci. Technol. 5, 3452–3458, 2015.

[40] M. Song, Q. Zhang, T. Liu, J. Yin, X. Guo, H. Zhang, X. Wang, First-principles study on electronic states of $SrWO_4$ crystals containing F-type color centers, Curr. Appl. Phys. 9, 812–815, 2009

[41] R. Lacomba-Perales, J. Ruiz-Fuertes, D. Errandonea, D. Martinez-Garcia and A. Segura, Optical absorption of divalent metal tungstates: Correlation between the band-gap energy and the cation ionic radius, Europhys. Lett. 83, 37002, 2008

[42] J. C. Sczancoski , W. Avansi , M. G. S. Costa , M. Siu Li , V. R. Mastelaro , R. S. Santos, E. Longo, L. S. Cavalcante, Effect of different strontium precursors on the growth process and optical properties of $SrWO_4$ microcrystals, J. Mater. Sci. 50, 8089–8103, 2015.

[43] Kubelka P, Munk F; Ein Beitrag zur optik der farbanstriche, Zeit. Techn. Phys. 12 593–601, 1931

[44] D. Chen, Z. Liu, S. Ouyang and J. Ye, Simple room-temperature mineralization method to $SrWO_4$ micro/nanostructures and their photocatalytic properties, J. Phys. Chem. C, 115, 15778–15784, 2011

[45] D. Errandonea, A. Muñoz, P. Rodríguez-Hernández, J. E. Proctor, F. Sapiña, and M. Bettinell, Theoretical and experimental study of the crystal Structures,lattice vibrations, and band structures of monazite-type $PbCrO_4$, $PbSeO_4$, $SrCrO_4$, and $SrSeO_4$, Inorg. Chem. 54, 7524–7535, 2015

[46] W. da Silva Pereira, M. Meneghetti Ferrer, G. Botelho, L. Gracia, I. Costa Nogueira, I. M. Pinatti, I. L. Viana Rosa, F. de Almeida La Porta, J. Andrés and E. Longo, Effects of chemical substitution on the structural and optical properties of α-$Ag_{2-2x}Ni_xWO_4$ ($0 \leq x \leq 0.08$) solid solutions, Phys. Chem. Chem. Phys. 18, 21966-21975, 2016

[47] S. K. Gupta, K. Sudarshan, A.P. Srivastava, R.M. Kadam, Visible light emission from bulk and nano $SrWO_4$: Possible role of defects in photoluminescence, J. Lumin. 192, 1220-1226, 2017

[48] Y. Zhang, N.A.W. Holzwarth, R.T. Williams, Electronic band structures of the scheelite materials $CaMoO_4$, $CaWO_4$, $PbMoO_4$, and $PbWO_4$, Phys. Rev. B, 57,12738–12750,1998

[49] L. E. Roy, D. Ortiz-Acosta, E. R. Batista, B. L. Scott, M. W. Blair, I. May, R. E. Del Sesto and R. L. Martin, Chem. Com. 46, 1848–1850, 2010.

[50] S. Ogo, H. Nakatsubo, K. Iwasaki, A. Sato, K. Murakami, T. Yabe, A. Ishikawa, H. Nakai, Y. Sekine, Electron-hopping brings lattice strain and high catalytic activity in the low-temperature oxidative coupling of methane in an electric field, J. Phys. Chem. 122, 2089–2096, 2018.

[51] F. A. Rabuffetti, S. P. Culver, L. Suescun, and R. L. Brutchey, Structural disorder in $AMoO_4$ (A = Ca, Sr, Ba) scheelite nanocrystals, Inorg. Chem. 53, 1056–1061, 2014

[52] S. K. Gupta, K. Sudarshan, P. S. Ghosh, K. Sanyal, A. P. Srivastava, A. Arya, P. K. Pujaria and R. M. Kadama, Luminescence of undoped and Eu^{3+} doped nanocrystalline $SrWO_4$ scheelite: time resolved fluorescence complimented by DFT and positron annihilation spectroscopic studies, RSC Adv. 6, 3792-3805, 2016

[53] Khang Hoang, Polaron formation, native defects and electronic conduction in metal tungstates, Phys. Rev. Mater. 1, 024603 (8 pages), 2017

[54] E. Orhan, M. Anicete-Santos, M. A. M. A. Maurera, F. M. Pontes, C. O. Paiva-Santos, A. G. Souza, J. A.Varela, P. S. Pizani, E. Longo, Conditions giving rise to intense visible room temperature photoluminescence in $SrWO_4$ thin films: the role of disorder, Chem. Phys., 312, 1-9, 2005

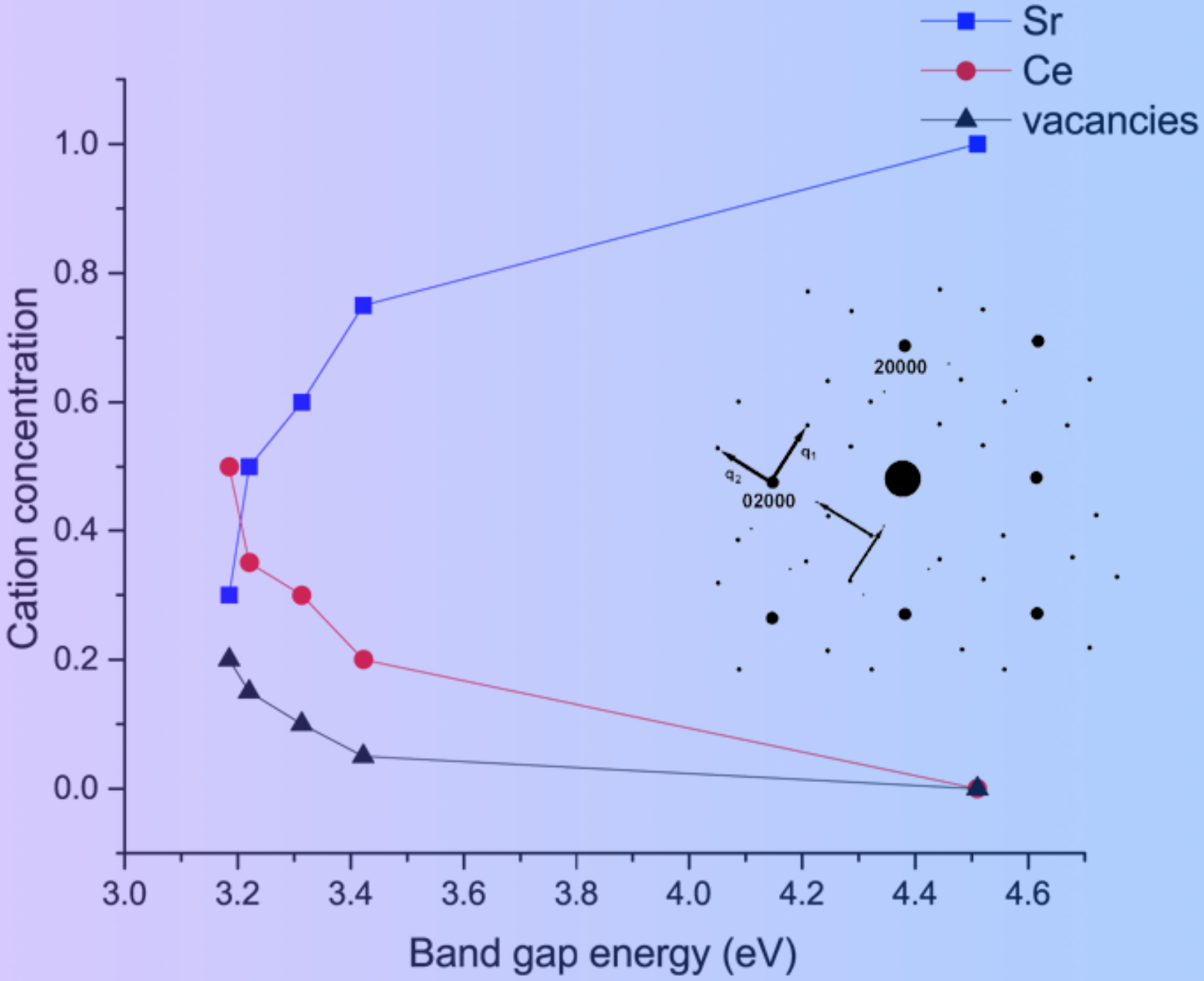
Sr
Ce
vacancies
Cation concentration
1.0
0.8
0.6
0.4
0.2
0.0
3.0
3.2
3.4
3.6
3.8
4.0
4.2
4.4
4.6
Band gap energy (eV)
20000
02000
q1
q2